2011 50th IEEE Conference on Decision and Control and
European Control Conference (CDC-ECC)
Orlando, FL, USA, December 12-15, 2011

Kernel mechanism of the cyanobacterial circadian clock is a relaxation oscillator

Lan Ma, Rama Ranganathan

Abstract—Circadian clock is an essential molecular regulatory mechanism that coordinates daily biological processes. Although the underlying design principles of eukaryotic circadian clock have been investigated in great detail, the circadian mechanism in cyanobacteria, the only prokaryote that possesses circadian clock, is not fully understood. In this study, we focus on elucidating the underlying systems property that drives the oscillation of the cyanobacterial clockwork. We apply combined methods of time scale separation, phase space analysis and bifurcation analysis to a model of circadian clock proposed by us recently. The original model is reduced to a three-dimensional slow subsystem by time scale separation. Phase space analysis of the reduced subsystem shows that the null-surface of the Serine-phosphorylated state (S state) of KaiC is a bistable surface and that the features of the phase portrait indicate that the kernel mechanism of the clockwork is a relaxation oscillator induced by positive and negative feedback loops. Bifurcation diagrams together with phase space analysis show that the S state of KaiC is a key component for the protein regulatory network of the cyanobacterial circadian clock.

INTRODUCTION

Diverse living organisms, from bacteria to humans, have developed complex molecular machinery of circadian clock to temporally coordinate internal biological processes of ~24hr cycle [1]. Proper functioning of circadian clock is crucial to the survival and health of host organisms. Cyanobacteria are the only prokaryote possessing circadian clock [2]. Three clock genes, namely KaiA, KaiB and KaiC, were identified to be essential for the cyanobacterial central oscillator [3]. Interestingly, self-sustained oscillatory phosphorylation of KaiC was reconstituted in vitro by mixing purified KaiA, KaiB and KaiC proteins at appropriate stoichiometry, together with ATP [4].

Mathematical modeling based on experiments has become a powerful approach to quantitatively explore dynamics of biological processes at systems level. Recently, we have proposed a mathematical model of the in vitro cyanobacterial circadian clock combining with experimental quantification, to account for the reactions of cyclic phosphorylation/dephosphorylation of the four KaiC phosphoforms as well as the association/dissociation reactions among species of Kai proteins (Figure 1) [5]. The model is represented by 10-dimensional (10-D) ordinary differential equations (ODE), describing the dynamics of monomeric KaiC phosphoforms in free (U, T, S, ST, denoting unphosphorylated KaiC, Threonine phosphorylated KaiC, Serine phosphorylated KaiC and Threonine & Serine doubly phosphorylated KaiC, respectively) and complex forms (UA, TA, SA, UAB, TAB, SAB, SB, denoting U, T, S in complex with KaiA and/or KaiB) (see Appendix for ODE). Computer simulations of the model have shown that it quantitatively agrees with the ordered phosphorylation of KaiC phosphoforms observed by other groups and the KaiB-C complexation measured by our FRET assay.

In this paper, we ask the following questions about the clock mechanism: what underlying systems property drives the oscillation of the cyanobacterial clockwork? Can we dissect the dynamical network of the oscillator and explore its embedding nonlinear features? Can we identify plausible key component(s) of the clock mechanism? Addressing these questions will enable us to deeply understand the molecular regulatory mechanism underlying circadian clock, which may lead to better therapeutic treatment to circadian mechanism in disease condition. To this end, we apply combined methods of time scale separation, phase space analysis and bifurcation analysis to our model of circadian clock. First, fast and slow timescales are separated, and under the classical quasi-steady state approximation of fast subsystem the model degenerates to a slow subsystem. Secondly, the 3-dimensional slow subsystem is subjected to phase space analysis and the phase portrait shows that the null-surface of the S-state is a bistable surface and that the

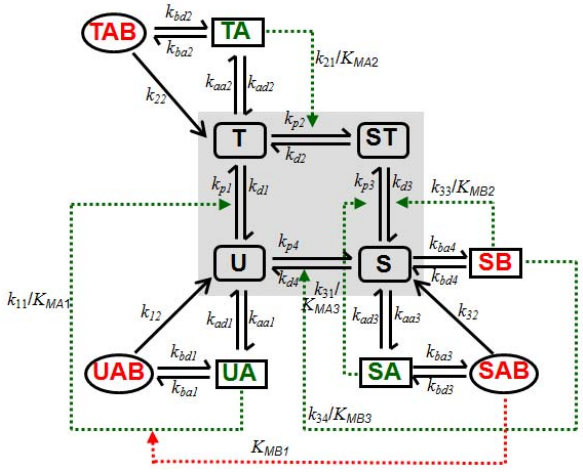

Fig. 1. Schematic diagram of our model of cyanobacterial circadian clock.

Lan Ma is with the Bioengineering Department, University of Texas at Dallas, 800 W Campbell Rd, EC39, Richardson, TX 75080, USA (e-mail: lan.ma@utdallas.edu).

Rama Ranganathan is with the Pharmacology Department, University of Texas Southwestern Medical Center, 5323 Harry Hines Blvd, Dallas, TX 75390, USA, (e-mail: rama.ranganathan@utsouthwestern.edu).

trait of the phase portrait of the reduced oscillator agrees with that of a relaxation oscillator. Thirdly, bifurcation plots together with phase space analysis indicate that the positive feedback loops are relatively more sensitive to perturbation than negative feedback loop. And both positive and negative feedback loops contribute to the bistable surface in the reduced phase space. Finally, we conclude that the Serine-phosphorylated state (S state) of KaiC is a key component for the protein regulatory network of the cyanobacterial circadian clock because the bistablity-induced oscillation stems from the phase surface of the S state.

RESULTS

A. Time scale separation and reduction of the model of KaiABC oscillator

To further analyze our model of circadian clock, the immediate difficulty we face is the high dimensionality of the dynamical system. By examining the model, we notice that the biochemical reactions underlying the in vitro cyanobacterial circadian oscillator undergo two different time scales: the phosphorylation and dephosphorylation of different KaiC phosphoforms are progressing slowly with time scale comparable to that of the circadian oscillation, while the association and dissociation among KaiA, KaiB and KaiC have relatively instantaneous reaction rates (>5-10 fold faster). For a multi-timescale biological system with both fast and slow reactions, the slow dynamics are typically dominating experimental observations. Thus it is eligible to apply singular perturbation theory [6] to generate reduced approximate slow subsystem, which is described by smaller number of state variables and amenable for efficient analysis and simulation. A classical example of such timescale analysis is the irreversible enzyme-catalyzed reaction, such as that of the Mechaelis-Menten. For our model of cyanobacterial circadian oscillator, the interconversions among U, T, ST and S inside the shaded area depicted in the model diagram (Figure 1) have slow rates, while the rest of reactions in the diagram occur relatively fast. Therefore, the fast state variables are identified as the seven KaiC species in complex with KaiA and KaiB, which are connected by those fast reaction rates of the model. That is, we define a fast vector x_f = [UA TA SA UAB TAB SAB SB], whose time rates of change are much larger than that of other variables. Then we can assume that these complexes of KaiC quickly settle at quasi-steady states, due to their instantaneous kinetics relative to the slow circadian dynamic with 24 hr periodicity. Based on the modified singular perturbation theory (see Appendix) and the subsequent quasi-steady state approximation, the original model can be reduced to a slow subsystem consisting of only three variables (i.e. any three species of U, T, ST and S due to conservation of KaiC concentration) that resides on the time-varying pseudo-equilibrium points of the fast subsystem. Because previous work has indicated plausible importance of the S-state of KaiC for the circadian clock, we decide to include S instead of ST in slow subsystem and subsequent analysis.

To derive the 3-dimensional subsystem mathematically, first we solve for the quasi-steady states of x_f by setting the derivatives d[UA]/dt, d[TA]/dt, d[SA]/dt, d[UAB]/dt, d[TAB]/dt, d[SAB]/dt and d[SB]/dt to zero. In addition, we assume that the fourth order sigmoid functions $\frac{[B]^4}{K_{Bi}^4+[B]^4}$ (i = 1-4) equals to one because [B], the concentration of free KaiB, is much bigger than K_{Bi}, the threshold constants for KaiB association. Then we analytically solve the following algebraic equations (1) for the quasi-steady states of the fast subsystem:

$$\begin{aligned}
&k_{aa1}[A]\cdot[U]-k_{ad1}[UA]-k_{ba1}[UA]+k_{bd1}[UAB]=0\\
&k_{aa2}[A]\cdot[T]-k_{ad2}[TA]-k_{ba2}[TA]+k_{bd2}[TAB]=0\\
&k_{aa3}[A]\cdot[S]-k_{ad3}[SA]-k_{ba3}[SA]+k_{bd3}[SAB]=0\\
&k_{ba1}[UA]-k_{bd1}[UAB]-k_{12}[UAB]=0\\
&k_{ba2}[TA]-k_{bd2}[TAB]-k_{22}[TAB]=0\\
&k_{ba3}[SA]-k_{bd3}[SAB]-k_{31}[SAB]=0\\
&k_{ba4}[S]-k_{bd4}[SB]=0
\end{aligned} \tag{1}$$

The quasi-steady state concentrations of the KaiC complexes are obtained as:

$$\begin{aligned}
[UA]&=\alpha_U[A][U]\\
[UAB]&=\alpha_U\beta_U[A][U]\\
[TA]&=\alpha_T[A][T]\\
[TAB]&=\alpha_T\beta_T[A][T]\\
[SA]&=\alpha_S[A][S]\\
[SAB]&=\alpha_S\beta_S[A][S]\\
[SB]&=\gamma_S[S]
\end{aligned}$$

where

$$\alpha_U=\frac{k_{aa1}}{k_{ad1}+k_{ba1}-k_{bd1}\frac{k_{ba1}}{k_{bd1}+k_{12}}},\quad \beta_U=\frac{k_{ba1}}{k_{bd1}+k_{12}}$$

$$\alpha_T=\frac{k_{aa2}}{k_{ad2}+k_{ba2}-k_{bd2}\frac{k_{ba2}}{k_{bd2}+k_{22}}},\quad \beta_T=\frac{k_{ba2}}{k_{bd2}+k_{22}}$$

$$\alpha_S=\frac{k_{aa3}(k_{bd3}+k_{31})}{k_{ad3}k_{bd3}+k_{ad3}k_{31}-k_{ba3}k_{31}},\quad \beta_S=\frac{k_{ba3}}{k_{bd3}+k_{31}},$$

$$\gamma_S=\frac{k_{ba4}}{k_{bd4}+k_{34}}$$

We see that the pseudo-equilibrium point of the fast subsystem depends on the slow variables and thus are time-varying. By substituting these pseudo-steady-state concentrations back into the slow subsystem d[U]/dt,

d[T]/dt, d[S]/dt, we then arrive at the final three-dimensional differential equations of the simplified system:

$$\frac{d[U]}{dt} = -k_{p1}[U] + k_{a1}[T] - k_{p4}[U] + k_{d4}[S] - k_{aa1}[A]\cdot[U] + k_{ad1}[UA] - k_{11}[U]\frac{[UA]}{K_{MA1}+[UA]}\cdot\frac{1}{1+([SAB]/K_{MB1})^4} + k_{12}[UAB] + k_{34}[S]\frac{[SB]^4}{K_{MB3}^4+[SB]^4}$$

$$\frac{d[T]}{dt} = k_{p1}[U] - k_{a1}[T] - k_{p2}[T] + k_{d2}[ST] - k_{aa2}[A]\cdot[T] + k_{ad2}[TA] - k_{21}[T]\frac{[TA]}{K_{MA2}+[TA]} + k_{11}[U]\frac{[UA]}{K_{MA1}+[UA]}\cdot\frac{1}{1+([SAB]/K_{MB1})^4} + k_{22}[TAB]$$

$$\frac{d[S]}{dt} = k_{d3}[ST] - k_{p3}[S] + k_{p4}[U] - k_{d4}[S] + k_{31}[SAB] - k_{aa3}[A][S] + k_{ad3}[SA] - k_{32}[S]\frac{[SA]}{K_{MA3}+[SA]} + k_{33}[ST]\frac{[SB]^4}{K_{MB2}^4+[SB]^4} - k_{ba4}[S]\frac{[B]^4}{K_{MB4}^4+[B]^4} + k_{bd4}[SB] - k_{34}[S]\frac{[SB]^4}{K_{MB3}^4+[SB]^4}$$

Note that we use S instead of ST in the 10-D ODE model as well as the resulting 3-D reduced model. Simulations show that the reduced system oscillates well, although with slightly smaller amplitude as well as periodicity (~22 hr) comparing to the original system (Figure 2).

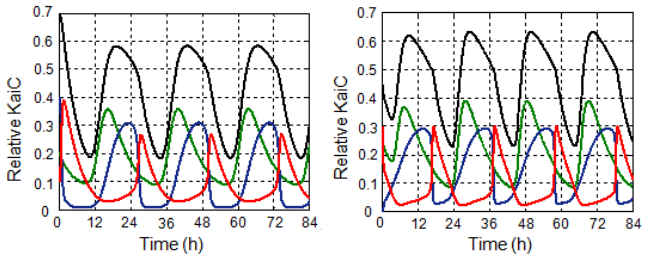

Fig. 2. Simulations of the original system (A) and reduced system (B). Time courses of phosphoform T, ST, S and total phosphorylated KaiC relative to total KaiC are represented by green, blue, red and black curves, respectively.

B. The simplified system is a relaxation oscillator

Phase portrait with nullclines and trajectories in 2-D phase plane is a standard method to analyze a 2-D dynamical nonlinear system. Now with the simplified 3-D clock model, we can analogously visualize its null-surfaces, instead of nullclines, in 3-D phase space. In order to do this, we set the right-hand-side of d[U]/dt, d[T]/dt and d[S]/dt to zero and solve for the solution numerically using MATLAB. The null-surfaces of U, T, S thus obtained are respectively denoted as P1, P2 and P3. As shown in Figure 3A, we notice that the P1 and P2 surfaces are almost flat while the P3 surface looks nonlinear. To get a better view of the surface of P3, we remove the P2 surface, which is nearly orthogonal to the U-T surface. By choosing an appropriate visual angle, we are able to see the P1 and P3 surfaces projected onto S-U surface (Figure 3B and 3C). Intriguingly, we find that the surface of P3 surface presents a rotated N- shaped feature,

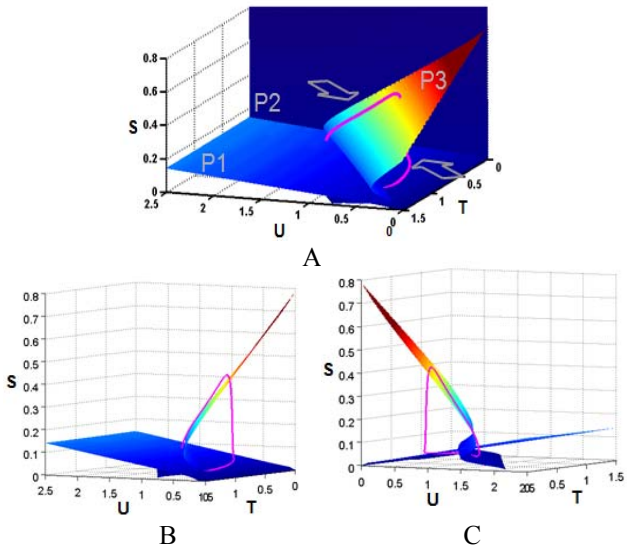

Fig. 3. Null-surfaces (P1, P2 and P3) of the reduced system. The purple line represents the trajectory.

and the linear surface of P1 surface intersects with the P3 surface at the intermediate portion of the N shape. It is well known that the hallmark of a typical 2D relaxation oscillator in phase portrait is that a linear nullcline (or the linear part of a nullcline) intersects with the middle/unstable branch of an N-shaped nullcline [7]. In addition, the limit cycle should orbit around the intersection of two nullclines, which is an unstable equilibrium point. For example, the famous Van der Pol oscillator has a straight-line nullcline intersecting with the other N-shaped nullcline at the middle branch [7]. The phase space plot of our reduced system shown in Figure 3 agrees well with these characteristics of a relaxation oscillator.

C. Perturbation of the oscillator

For a 2D relaxation oscillator, the oscillation is destroyed if the fixed point shifts outside of the middle (unstable) branch of the N-shaped nullcline. One famous example is the "excitation block" phenomenon explained by the FitzHugh-Nagumo model [8]. To see if our model presents such type of behavior, we first perform bifurcation analysis of the full system. In each bifurcation plot, a single parameter value is perturbed and the dynamical response is plotted at the perturbed value. Such bifurcation plots are shown for parameters k11, k21, k31, k33, kaa3, kba3 and kba4 (Figure 4), where k11 and k21 are rates regulating negative feedback loops, k31, kaa3, kba3 and kba4 are rates regulating positive feedback loops, and k33 is rate shared by negative and positive feedback loops (Figure 3). By defining the robustness index (RI) as the ratio between the upper bound and lower bound of the oscillatory region, we have RI(k11)=141, RI(k21)=∞, RI(k31)=7.14, RI(kaa3)=4.7, RI(kba3)=6.8, RI(kba4)=2.3, RI(k33)=33. The larger the RI value, the more robust for the system with respect to that parameter. Note that the degree of robustness of the two

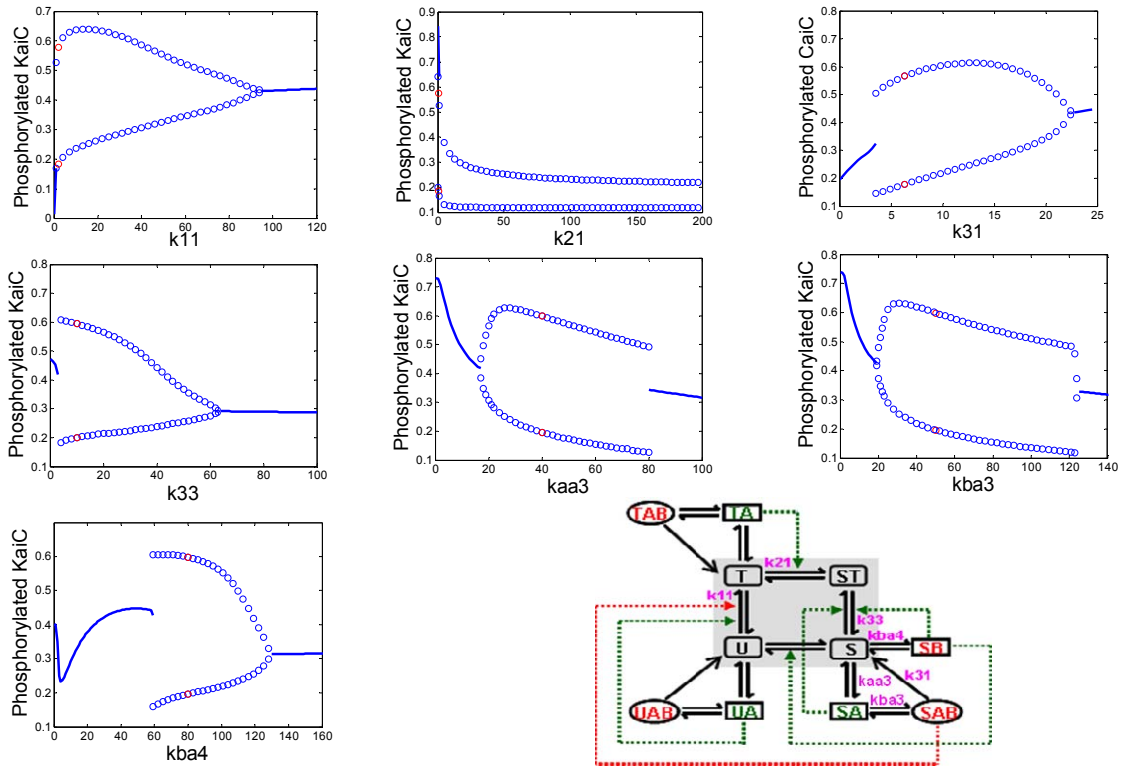

Fig. 4. Single-parameter bifurcation diagrams. Steady-state behavior of the model is plotted vs. a parameter selected from positive and negative feedback loops. Oscillation is represented by a pair of circles, while equilibrium point is represented by solid line. The nominal behavior is represented by a pair of red circles.

rates associated with negative feedback loop (k11 and k21) is much higher than that of the rates associated with positive feedback loops (k31, kaa3, kba3 and kba4).

How do the perturbations of parameters affect the reduced system in the phase plot? For each of the above parameters, we choose a value right outside the oscillatory region and compare the 3-dimensional null-surfaces of the perturbed (non-oscillatory) and unperturbed (oscillatory) model (Figure 5). Indicating the shift of surfaces by red arrows, Figure 5 shows that under parameter perturbations the conformation of one or more null-surfaces changes. The shift of P2 surface seems to have the least effect on the system dynamics because increased k21 does not abolish the oscillation, which tilts P2 surface while P1 and P3 remain the same (data not shown). The shift of the P3 surface is induced by three parameters (k33, kba4, kaa3) associated immediately with the S-state of KaiC in the network, indicating that the N-shaped bistability surfaces stems from the direct regulations of the S-state. This result underscores the importance of the S-state because the N-shaped null-surface/nullcline is the core of a relaxation oscillator. These phase space perturbation plots show that the robustness of our oscillatory model essentially is determined by the conformation of the null-surfaces. But how the conformation of the 3D null-surfaces determines the oscillation of system is still unclear. Since the oscillation of the system seems to be insensitive to the perturbation in P2 surface, we eliminate this degree of freedom by solving the intersections of P1 and P3 on P2. As shown in Figure 6, the intersection between P1 and P2 is a straight line except near the origin, while the intersection between P1 and P3 is an N-shaped curve. These intersection curves on P2 surface have the characteristics of nullclines of a 2-D relaxation oscillator. Moreover, we find that for the nominal oscillatory model the fixed point (intersect of P1, P2 and P3) is on the middle branch of the N-shaped curve, while the oscillation is disabled if the fixed point sits outside of the middle branch of the N-shaped curve. That is, the fixed point has to lie on the middle branch of the N-shaped curve to be an unstable fixed point. Such behavior again agrees well with that of a 2-D relaxation oscillator. The above phase plots combined with perturbation analysis suggests that the kernel mechanism of our model of circadian clock is a relaxation oscillator.

CONCLUSION

In the schematic diagram of the full model, the S-state is a hub element of two positive feedbacks and a negative feedback loop, which indicates that the S-state is a critical component for the functioning of the circadian oscillator. Our phase surface analysis together with bifurcation diagrams show that the nonlinearity associated with the null-surface of the S-state is critical for the simplified relaxation oscillator, highlighting the important role of the S-state of KaiC in the cyanobacterial circadian mechanism.

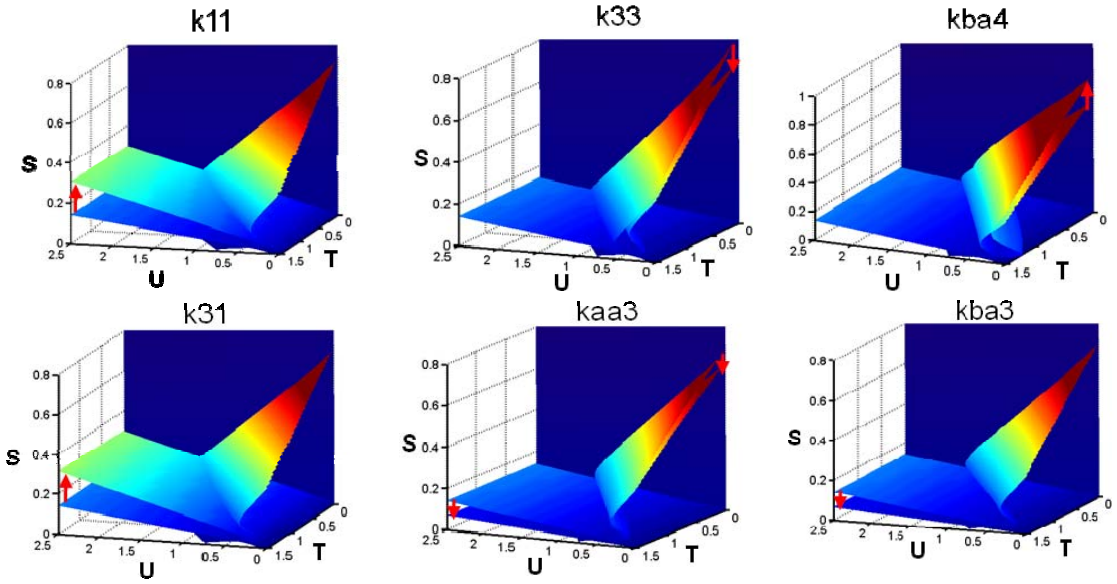

Fig. 5. Nullplanes before and after perturbation of the parameter listed above each plot. The red arrow indicates the direction from unperturbed to perturbed situation.

APPENDIX

The 10-D ODE model of circadian clock is given as:

$$\frac{d[\mathrm{U}]}{dt} = -k_{p1}[\mathrm{U}] + k_{d1}[\mathrm{T}] - k_{p4}[\mathrm{U}] + k_{d4}[\mathrm{S}] - k_{aa1}[\mathrm{A}]\cdot[\mathrm{U}] + k_{ad1}[\mathrm{UA}] - k_{11}[\mathrm{U}]\frac{[\mathrm{UA}]}{K_{MA1}+[\mathrm{UA}]}\cdot\frac{1}{1+([\mathrm{SAB}]/K_{MB1})^4} + k_{12}[\mathrm{UAB}] + k_{34}[\mathrm{S}]\frac{[\mathrm{SB}]^4}{K_{MB3}^4+[\mathrm{SB}]^4}$$

$$\frac{d[\mathrm{T}]}{dt} = k_{p1}[\mathrm{U}] - k_{d1}[\mathrm{T}] - k_{p2}[\mathrm{T}] + k_{d2}[\mathrm{ST}] - k_{aa2}[\mathrm{A}]\cdot[\mathrm{T}] + k_{ad2}[\mathrm{TA}] - k_{21}[\mathrm{T}]\frac{[\mathrm{TA}]}{K_{MA2}+[\mathrm{TA}]} + k_{22}[\mathrm{TAB}] + k_{11}[\mathrm{U}]\frac{[\mathrm{UA}]}{K_{MA1}+[\mathrm{UA}]}\cdot\frac{1}{1+([\mathrm{SAB}]/K_{MB1})^4}$$

$$\frac{d[\mathrm{ST}]}{dt} = k_{p2}[\mathrm{T}] - k_{d2}[\mathrm{ST}] - k_{d3}[\mathrm{ST}] + k_{p3}[\mathrm{S}] + k_{21}[\mathrm{T}]\frac{[\mathrm{TA}]}{K_{M2}+[\mathrm{TA}]} + k_{32}[\mathrm{S}]\frac{[\mathrm{SA}]}{K_{MA3}+[\mathrm{SA}]} - k_{33}[\mathrm{ST}]\frac{[\mathrm{SB}]^4}{K_{MB2}^4+[\mathrm{SB}]^4}$$

$$\frac{d[\mathrm{UA}]}{dt} = k_{aa1}[\mathrm{A}]\cdot[\mathrm{U}] - k_{ad1}[\mathrm{UA}] - k_{ba1}[\mathrm{UA}]\frac{[\mathrm{B}]^4}{K_{B1}^4+[\mathrm{B}]^4} + k_{bd1}[\mathrm{UAB}]$$

$$\frac{d[\mathrm{TA}]}{dt} = k_{aa2}[\mathrm{A}]\cdot[\mathrm{T}] - k_{ad2}[\mathrm{TA}] - k_{ba2}[\mathrm{TA}]\frac{[\mathrm{B}]^4}{K_{B2}^4+[\mathrm{B}]^4} + k_{bd2}[\mathrm{TAB}]$$

$$\frac{d[\mathrm{SA}]}{dt} = k_{aa3}[\mathrm{A}]\cdot[\mathrm{S}] - k_{ad3}[\mathrm{SA}] - k_{ba3}[\mathrm{SA}]\frac{[\mathrm{B}]^4}{K_{B3}^4+[\mathrm{B}]^4} + k_{bd3}[\mathrm{SAB}]$$

$$\frac{d[\mathrm{UAB}]}{dt} = k_{ba1}[\mathrm{UA}]\frac{[\mathrm{B}]^4}{K_{B1}^4+[\mathrm{B}]^4} - k_{bd1}[\mathrm{UAB}] - k_{12}[\mathrm{UAB}]$$

$$\frac{d[\mathrm{TAB}]}{dt} = k_{ba2}[\mathrm{TA}]\frac{[\mathrm{B}]^4}{K_{B2}^4+[\mathrm{B}]^4} - k_{bd2}[\mathrm{TAB}] - k_{22}[\mathrm{TAB}]$$

$$\frac{d[\mathrm{SAB}]}{dt} = k_{ba3}[\mathrm{SA}]\frac{[\mathrm{B}]^4}{K_{B3}^4+[\mathrm{B}]^4} - k_{bd3}[\mathrm{SAB}] - k_{31}[\mathrm{SAB}]$$

$$\frac{d[\mathrm{SB}]}{dt} = k_{ba4}[\mathrm{S}]\frac{[\mathrm{B}]^4}{K_{B4}^4+[\mathrm{B}]^4} - k_{bd4}[\mathrm{SB}]$$

And the eleventh KaiC species S is constrained by the conservation of the total concentration of KaiC, i.e., [U] + [T] + [ST] + [UA] + [TA] + [SA] + [UAB] + [TAB] + [SAB] + [SB] + [S] = $\mathrm{KaiC}^{\mathrm{T}}$. The method of model reduction we use is based on singular perturbation theory [6]. Suppose a dynamical system has separable fast and slow variables, denoted by x_s and x_f, respectively. Due to the slow/fast time rate of change for slow/fast variables, the state-space representation of the model is represented as:

$$\dot{x}_s = f(t, x_s, x_f, \varepsilon), \qquad x_s \in R^n \qquad (2)$$

$$\varepsilon \cdot \dot{x}_f = g(t, x_s, x_f, \varepsilon), \qquad x_f \in R^m \qquad (3)$$

where $\varepsilon << 1$ is a small positive parameter and f and g are continuously differentiable functions. On the time scale that slow variables show variation, the fast variables quickly settle to their quasi-steady-state if the fast subsystem has at least one isolated real roots. This leads to the standard singular perturbation theory that sets $\varepsilon = 0$ and the dimension of the original system reduces from $m+n$ to n because the differential equation (3) degenerates to algebraic equation:

$$0 = g(t, x_s, x_f^0, 0) \quad (4)$$

Here we use a modified singular perturbation model that has improved accuracy [9]. Using such a model, we do not set ε to 0 and the reduced slow subsystem becomes

$$\dot{x}_s = f(t, x_s, h(t,x), \varepsilon) \qquad (5)$$

where $h(t, x)$ is the steady-state solution for x_f^0 in the following algebraic equation:

$$0 = g(t, x_s, x_f^0, \varepsilon) \quad (6)$$

For our model of KaiABC oscillator, the association and dissociation rates among the Kai proteins (k_{aai} and k_{adi}, i=1-3; k_{baj} and k_{bdj}, j=1-4) are much bigger (~13-80000 fold) than

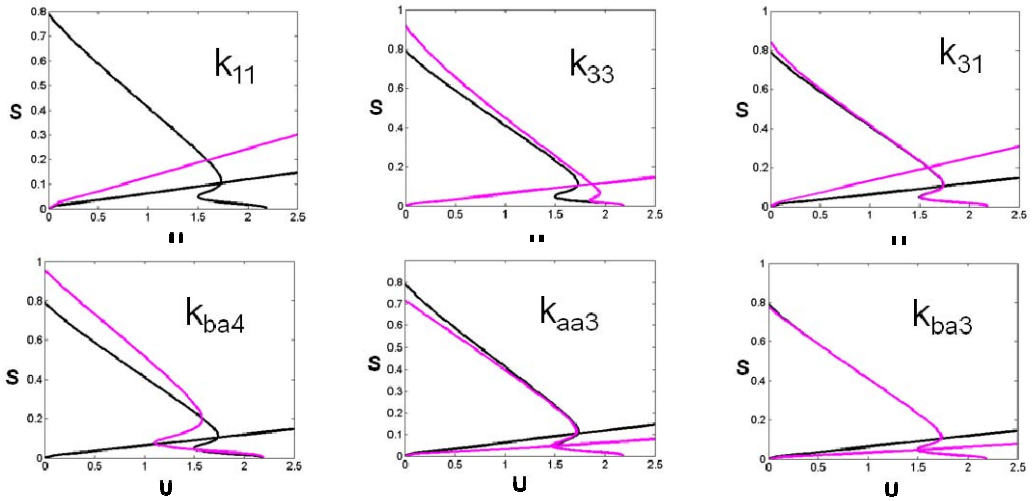

Fig. 6. Null-surfaces P1 and P3 projected onto P2 before (black) and after (magenta) the perturbation of the parameter listed in each plot.

the phosphorylation and dephosphorylation rates (k_{pl} and k_{dl}, l=1-4, and k_{11}, k_{12}, k_{21}, k_{22}, k_{32}, k_{33} and k_{34}). And the derivative of the fast variables x_f= [[UA] [TA] [SA] [UAB] [TAB] [SAB] [SB]] is dominated by the fast binding reactions. That is, if we rewrite $k_{aai} = 1/\varepsilon\ k^*_{aai}$, $k_{adi} = 1/\varepsilon k^*_{adi}$, i =1-3, and $k_{baj} = 1/\varepsilon k^*_{baj}$, $k_{bdj} = 1/\varepsilon k^*_{bdj}$, j=1-4, with the choice of ε = 0.08 (i.e. 1/12.5), the differential equation for the fast subsystem then takes the standard form in (3), where the vector field g is:

$$g = \begin{bmatrix} k^*_{aa1}[\mathrm{A}]\cdot[\mathrm{U}] - k^*_{ad1}[\mathrm{UA}] - k^*_{ba1}[\mathrm{UA}]\dfrac{[\mathrm{B}]^4}{K^4_{B1}+[\mathrm{B}]^4} + k^*_{bd1}[\mathrm{UAB}] \\ k^*_{aa2}[\mathrm{A}]\cdot[\mathrm{T}] - k^*_{ad2}[\mathrm{TA}] - k^*_{ba2}[\mathrm{TA}]\dfrac{[\mathrm{B}]^4}{K^4_{B2}+[\mathrm{B}]^4} + k^*_{bd2}[\mathrm{TAB}] \\ k^*_{aa3}[\mathrm{A}]\cdot[\mathrm{S}] - k^*_{ad3}[\mathrm{SA}] - k^*_{ba3}[\mathrm{SA}]\dfrac{[\mathrm{B}]^4}{K^4_{B3}+[\mathrm{B}]^4} + k^*_{bd3}[\mathrm{SAB}] \\ k^*_{ba1}[\mathrm{UA}]\dfrac{[\mathrm{B}]^4}{K^4_{B1}+[\mathrm{B}]^4} - k^*_{bd1}[\mathrm{UAB}] - \varepsilon\cdot k_{12}[\mathrm{UAB}] \\ k^*_{ba2}[\mathrm{TA}]\dfrac{[\mathrm{B}]^4}{K^4_{B2}+[\mathrm{B}]^4} - k^*_{bd2}[\mathrm{TAB}] - \varepsilon\cdot k_{22}[\mathrm{TAB}] \\ k^*_{ba3}[\mathrm{SA}]\dfrac{[\mathrm{B}]^4}{K^4_{B3}+[\mathrm{B}]^4} - k^*_{bd3}[\mathrm{SAB}] - \varepsilon\cdot k_{31}[\mathrm{SAB}] \\ k^*_{ba4}[\mathrm{S}]\dfrac{[\mathrm{B}]^4}{K^4_{B4}+[\mathrm{B}]^4} - k^*_{bd4}[\mathrm{SB}] \end{bmatrix}$$

Note that the order of derivatives on the left-hand sides of equation (3) is not affected by the terms multiplied by ε on the right-hand side because they can be neglected in comparison with the other right-hand-side terms. Next we examine the slow subsystem of KaiABC oscillator with variable x_s = [[U] [T] [S]]. Here we have chosen to explicitly include the S-state of KaiC instead of the ST-state in the slow variables because our previous study indicates that the S phorylated-state of KaiC is likely a critical component in determining the dynamics of the circadian oscillator. Based on the differential equations of x_s, it is noteworthy that the derivatives of x_s are dominated by terms of slow phosphorylation/dephosphorylation reactions, except for one or two paired association/dissociation reactions. Since the latter are equilibrated quickly, the net rate of these reaction pairs turn out to be in the same order of magnitude as the rest of the slow terms (simulation not shown).

ACKNOWLEDGMENT

The authors are grateful for the Start-up Fund from the University of Texas at Dallas.

REFERENCES

1. Bell-Pedersen, D., et al., *Circadian rhythms from multiple oscillators: lessons from diverse organisms.* Nat Rev Genet, 2005. 6(7): p. 544-56.
2. Golden, S.S., et al., *Cyanobacterial Circadian Rhythms.* Annu Rev Plant Physiol Plant Mol Biol, 1997. 48: p. 327-354.
3. Ishiura, M., et al., *Expression of a gene cluster kaiABC as a circadian feedback process in cyanobacteria.* Science, 1998. 281(5382): p. 1519-23.
4. Nakajima, M., et al., *Reconstitution of circadian oscillation of cyanobacterial KaiC phosphorylation in vitro.* Science, 2005. 308(5720): p. 414-5.
5. Ma, L., and Ranganathan, R., *Quantifying the rhythm of KaiB-C complexation for in vitro cyanobacterial circadian clock.* Under revision.
6. Khalil, H.K., *Nonlinear systems*. 1996, Upper Saddle River, NJ: Prentice Hall.
7. Strogatz, S., *Nonlinear dynamics and chaos: with applications to physics, biology, chemistry and engineering*. 2001: Westview Press.
8. Keener, J., J. Sneyd *Mathematical Physiology*. 1998: Springer-Verlag
9. Gomez-Uribe, C.A., G.C. Verghese, and A.R. Tzafriri, *Enhanced identification and exploitation of time scales for model reduction in stochastic chemical kinetics.* J Chem Phys, 2008. 129(24): p. 244112.